1098 *Chem. Mater.* **2010,** *22,* 1098–1106
DOI:10.1021/cm902218j

CHEMISTRY OF MATERIALS
Article

Synthesis and Oxygen Reduction Electrocatalytic Property of Platinum Hollow and Platinum-on-Silver Nanoparticles†

Zhenmeng Peng, Jianbo Wu, and Hong Yang*

Department of Chemical Engineering, University of Rochester, Gavett Hall 206, Rochester, New York 14627-0166

Received July 20, 2009. Revised Manuscript Received September 2, 2009

Pt-on-Ag bimetallic nanoparticles were prepared based on a heterogeneous nucleation and growth method. Interestingly, platinum hollow nanoparticles could be obtained by selectively removing the silver cores from Pt-on-Ag nanoparticles. High-resolution transmission electron microscopy (HR-TEM), energy-dispersive X-ray (EDX) analysis with a high-angle annular dark-field scanning transmission electron microscope (HAADF-STEM), and X-ray diffraction (XRD) were used to characterize these nanostructures. The observation that Pt hollows can be produced from Pt-on-Ag nanoparticles through the dissolution of Ag metal cores indicates that particle-on-particle nanodendrites were most likely derived from the products formed through the Stranski−Krastanov (SK) growth. The carbon-supported Pt hollow catalysts, which possessed much higher catalytic activity in oxygen reduction reaction (ORR) than the Pt-on-Ag nanoparticles, were also better than a commercial Pt catalyst (E-tek, 20% Pt). The nanometer-sized textures of the wall of Pt hollow spheres could contribute to the enhancement of the electrocatalytic activity.

Introduction

Platinum is the most widely used electrocatalyst in proton exchange membrane fuel cells (PEMFCs), especially for vehicle power applications using hydrogen fuel cells.[1−4] A challenge that needs to be overcome is the slow kinetics of oxygen reduction reaction (ORR) catalyzed by nanometer (nm)-sized Pt metal particles in the cathode membranes. While the mass current density of Pt catalysts for hydrogen fuel cells has improved dramatically during the past several years, further development is still urgently needed.[5,6] In this context, design of novel platinum nanostructures has been the research focus of many scientists in search of next generation high-performance electrocatalysts.[1,2,7−14]

Two areas have attracted particular attentions recently in the development of platinum-based cathode catalysts. Enhanced activity and improved stability in catalyzing ORR by Pt-on-Pd heteronanostructures or nanodendrites have been reported.[12,15] The synthesis of such catalysts begins with the production of core Pd nanoparticles through the colloidal synthesis. Platinum nanoparticles grow subsequently onto the Pd core nanoparticles from molecular species.[16−18] Besides Pt−Pd bimetallics, a few other Pt-on-M (M = metal) heterogeneous nanoparticles have also been synthesized, and some have been tested for their electrocatalytic performance.[19−21] Another intriguing new class of Pt-based electrocatalysts is porous nanostructures which include tubes, hollows, porous dendrites and networks. Both Pt nanotubes and hollow spheres have been made and demonstrated to have higher

† Accepted as part of the 2010 "Materials Chemistry of Energy Conversion Special Issue".

*Corresponding author. Telephone: (585) 275-2110. Fax: (585) 273-1348. E-mail: hongyang@che.rochester.edu.

(1) Peng, Z. M.; Yang, H. *Nano Today* **2009**, *4*, 143–164.
(2) Gasteiger, H. A.; Kocha, S. S.; Sompalli, B.; Wagner, F. T. *Appl. Catal., B* **2005**, *56*, 9–35.
(3) Lovic, J. D.; Tripkovic, A. V.; Gojkovic, S. L. J.; Popovic, K. D.; Tripkovic, D. V.; Olszewski, P.; Kowal, A. *J. Electroanal. Chem.* **2005**, *581*, 294–302.
(4) Chen, J. Y.; Lim, B.; Lee, E. P.; Xia, Y. N. *Nano Today* **2009**, *4*, 81–95.
(5) de Bruijn, F. A.; Dam, V. A. T.; Janssen, G. J. M. *Fuel Cells* **2008**, *8*, 3–22.
(6) Ferreira, P. J.; la, O, G. J.; Shao-Horn, Y.; Morgan, D.; Makharia, R.; Kocha, S.; Gasteiger, H. A. *J. Electrochem. Soc.* **2005**, *152*, A2256–A2271.
(7) Zhong, C. J.; Luo, J.; Njoki, P. N.; Mott, D.; Wanjala, B.; Loukrakpam, R.; Lim, S.; Wang, L.; Fang, B.; Xu, Z. C. *Energy Environ. Sci.* **2008**, *1*, 454–466.
(8) Zhang, J. L.; Mo, Y.; Vukmirovic, M. B.; Klie, R.; Sasaki, K.; Adzic, R. R. *J. Phys. Chem. B* **2004**, *108*, 10955–10964.
(9) Zhang, J. L.; Sasaki, K.; Sutter, E.; Adzic, R. R. *Science* **2007**, *315*, 220–222.
(10) Stamenkovic, V. R.; Fowler, B.; Mun, B. S.; Wang, G. F.; Ross, P. N.; Lucas, C. A.; Markovic, N. M. *Science* **2007**, *315*, 493–497.
(11) Koh, S.; Strasser, P. *J. Am. Chem. Soc.* **2007**, *129*, 12624–12625.
(12) Peng, Z. M.; Yang, H. *J. Am. Chem. Soc.* **2009**, *131*, 7542–7543.
(13) Lee, E. P.; Peng, Z. M.; Cate, D. M.; Yang, H.; Campbell, C. T.; Xia, Y. *J. Am. Chem. Soc.* **2007**, *129*, 10634–10635.
(14) Lee, E. P.; Peng, Z. M.; Chen, W.; Chen, S. W.; Yang, H.; Xia, Y. N. *ACS Nano* **2008**, *2*, 2167–2173.
(15) Lim, B.; Jiang, M. J.; Camargo, P. H. C.; Cho, E. C.; Tao, J.; Lu, X. M.; Xia, Y. N. *Science* **2009**, *324*, 1302–1305.
(16) Tao, F.; Grass, M. E.; Zhang, Y. W.; Butcher, D. R.; Renzas, J. R.; Liu, Z.; Chung, J. Y.; Mun, B. S.; Salmeron, M.; Somorjai, G. A. *Science* **2008**, *322*, 932–934.
(17) Guo, Q. J.; Teng, X. W.; Yang, H. *Adv. Mater.* **2004**, *16*, 1337–1341.
(18) Teng, X. W.; Yang, H. *J. Am. Chem. Soc.* **2003**, *125*, 14559–14563.
(19) Peng, Z. M.; Yang, H. *Nano Res.* **2009**, *2*, 406–415.
(20) Zhou, S. G.; McIlwrath, K.; Jackson, G.; Eichhorn, B. *J. Am. Chem. Soc.* **2006**, *128*, 1780–1781.
(21) Beard, K. D.; Borrelli, D.; Cramer, A. M.; Blom, D.; Zee, J. W. V.; Monnier, J. R. ACS Nano **2009**, DOI: 10.1021/nn900214g.

Published on Web 09/24/2009

ORR activities than pure Pt particles.[22,23] Besides ORR reduction, some of these Pt nanostructures possess very good catalytic property in methanol oxidation reaction (MOR).[24−26] Hollow and porous nanostructures of platinum bimetals and alloys have also been studied, and in some systems excellent catalytic properties have been found.[25,27−32]

In this paper we present the design and synthesis of Pt-on-Ag heterogeneous nanostructures and their applications in the preparation of a new kind of Pt hollow spheres consisting of continuous interconnected fine primary nanoparticles. Unlike the commonly used galvanic replacement method,[28,29,33−35] these hollow nanostructures were prepared through a selective removal of silver cores. The platinum hollow structures can be controlled very well and show superior activity in ORR when compared with the commercial Pt catalysts. The PtAg mixed nanoalloys made from Pt-on-Ag nanoparticles through thermal treatment, on the other hand, had a much worse ORR activity than the same reference Pt catalyst.

Experimental Section

Synthesis. The Pt-on-Ag bimetallic heterogeneous nanoparticles were prepared using a sequential synthetic method,[12,36,37] which involved the generation of silver nanoparticles in organic mixtures and then the deposition of platinum metal. Air and water dissolved in the mixtures were removed by a vacuum pump and a flow of argon gas was used during the synthesis.

Preparation of Silver Nanoparticles. The 9.5-nm silver nanoparticles were prepared using a modified procedure published elsewhere.[38] Specifically, silver trifluoroacetate (AgTFA, 98%, Aldrich, 0.22 g or 1 mmol) was mixed with oleylamine (OAm, 70%, Aldrich, 0.99 mL or 3 mmol) and isoamyl ether (99%, Aldrich, 5 mL) in a 25-mL three-neck flask and slowly heated to 160 °C in an oil bath in 80 min. The reaction was kept at this temperature for 90 min. The product was washed with 10 mL of ethanol, followed by centrifugation at 4000 rpm for 5 min. The precipitate was washed one additional time with 5 mL of ethanol and then redispersed in 10 mL of diphenyl ether (DPE, 99%, Aldrich).

Preparation of Pt-on-Ag Bimetallic Heteronanostructures. Platinum was deposited onto surfaces of as-prepared Ag nanoparticles to produce Pt-on-Ag bimetallic heteronanostructures. In a typical procedure, a dispersion of Ag nanoparticles (50 μmol Ag metal) in DPE was added into a solution of platinum acetylacetonate ($Pt(acac)_2$, 98%, Strem, 0.02 g or 50 μmol), OAm (0.3 mL or 0.9 mmol), and DPE in a 25-mL three-neck flask. The total volume of DPE was fixed at 5 mL for all experiments. The mole number of metals added was determined by thermal gravimetric analysis (TGA) conducted on an SDT-Q600 system from TA Instruments, Inc. The mixture was heated to 180 °C using an oil bath and kept at this temperature for 1 h unless stated otherwise. The product was washed and precipitated out by adding 10 mL of ethanol as the antisolvent and centrifugation at 6000 rpm for 5 min. The precipitate was collected and dispersed in 2 mL of toluene. To study the effects of key reaction conditions on the formation of Pt-on-Ag heteronanostructures, we varied the amount of Ag nanoparticles used between 25 to 100 μmol, reaction temperature from 170 to 190 °C, and reaction time from 2 min to 2 h. Only one variable was adjusted each time while all other conditions were kept the same.

Preparation of Carbon-Supported Pt-on-Ag Nanoparticles. Carbon black (Vulcan XC-72) was used to support as-prepared Pt-on-Ag nanoparticles before any further treatment. In a typical procedure, 50 mg of carbon black was dispersed in 5 mL of toluene and sonicated for 1 h before the addition of Pt-on-Ag nanoparticles in toluene. The amount of Pt-on-Ag nanoparticles was predetermined using TGA analysis and fixed at 15 wt % of the final product. The mixed dispersions were stirred overnight before being collected via centrifugation at 6000 rpm for 5 min. The precipitate was allowed to dry at room temperature under ambient conditions.

Thermal treatment of carbon-supported Pt-on-Ag bimetallic nanoparticles. Two different procedures were used to remove surface capping agents on the Pt-on-Ag nanoparticles for the preparation of catalyst. One was an acid-based treatment used for the removal of surfactants on palladium nanoparticles.[39] To be specific, 30 mg of carbon-supported Pt-on-Ag nanoparticles were added into 10 mL of acetic acid and heated for 10 h at 70 °C, where acetic acid reacted with the capped surfactants. The reaction mixture was cooled down to room temperature and washed for three times with 20 mL of ethanol, followed by centrifugation at 6000 rpm for 5 min. This procedure was repeated once with ethanol instead of acetone. The resulting product was dried at room temperature under ambient conditions. Alternatively, 30 mg of carbon-supported Pt-on-Ag nanoparticles was heated to 300 °C in air at a ramping rate of 2 °C/min and held at that temperature for 1 h in a tube furnace (Lindberg/Blue, Mini-Lite).[12,19] The product was further treated at 300 °C for 1 h under a reductive atmosphere of 5 vol % hydrogen in argon. With this thermal treatment, the Pt-on-Ag bimetallic nanoparticles turned into PtAg mixed nanoalloys.

Preparation of Pt Hollow Nanostructures. Pt hollow nanostructures were made via a selective removal of Ag metal from the Pt-on-Ag nanoparticles electrochemically. The experiment was conducted in a 125-mL five-neck flask using a CHI 760 dual channel electrochemical workstation (CH Instruments, Inc.).

(22) Chen, Z. W.; Waje, M.; Li, W. Z.; Yan, Y. S. *Angew. Chem., Int. Ed.* **2007**, *46*, 4060–4063.
(23) Chen, H. M.; Liu, R. S.; Lo, M. Y.; Chang, S. C.; Tsai, L. D.; Peng, Y. M.; Lee, J. F. *J. Phys. Chem. C* **2008**, *112*, 7522–7526.
(24) Liang, H. P.; Zhang, H. M.; Hu, J. S.; Guo, Y. G.; Wan, L. J.; Bai, C. L. *Angew. Chem., Int. Ed.* **2004**, *43*, 1540–1543.
(25) Guo, S. J.; Dong, S. J.; Wang, E. *Chem.—Eur. J.* **2008**, *14*, 4689–4695.
(26) Teng, X. W.; Liang, X. Y.; Maksimuk, S.; Yang, H. *Small* **2006**, *2*, 249–253.
(27) Liang, H. P.; Guo, Y. G.; Zhang, H. M.; Hu, J. S.; Wan, L. J.; Bai, C. L. *Chem. Commun.* **2004**, 1496–1497.
(28) Chen, G.; Xia, D. G.; Nie, Z. R.; Wang, Z. Y.; Wang, L.; Zhang, L.; Zhang, J. J. *Chem. Mater.* **2007**, *19*, 1840–1844.
(29) Vasquez, Y.; Sra, A. K.; Schaak, R. E. *J. Am. Chem. Soc.* **2005**, *127*, 12504–12505.
(30) Teng, X. W.; Maksimuk, S.; Frommer, S.; Yang, H. *Chem. Mater.* **2007**, *19*, 36–41.
(31) Ding, Y.; Chen, M. W.; Erlebacher, J. *J. Am. Chem. Soc.* **2004**, *126*, 6876–6877.
(32) Xu, C. X.; Wang, L. Q.; Wang, R. Y.; Wang, K.; Zhang, Y.; Tian, F.; Ding, Y. *Adv. Mater.* **2009**, *21*, 2165–2169.
(33) Mayers, B.; Jiang, X. C.; Sunderland, D.; Cattle, B.; Xia, Y. N. *J. Am. Chem. Soc.* **2003**, *125*, 13364–13365.
(34) Sun, Y. G.; Mayers, B.; Xia, Y. N. *Adv. Mater.* **2003**, *15*, 641–646.
(35) Sun, Y. G.; Mayers, B. T.; Xia, Y. N. *Nano Lett.* **2002**, *2*, 481–485.
(36) Teng, X. W.; Black, D.; Watkins, N. J.; Gao, Y. L.; Yang, H. *Nano Lett.* **2003**, *3*, 261–264.
(37) Lee, H. J.; Habas, S. E.; Somorjai, G. A.; Yang, P. D. *J. Am. Chem. Soc.* **2008**, *130*, 5406–5407.
(38) Lu, X. M.; Tuan, H. Y.; Chen, J. Y.; Li, Z. Y.; Korgel, B. A.; Xia, Y. N. *J. Am. Chem. Soc.* **2007**, *129*, 1733–1742.
(39) Mazumder, V.; Sun, S. H. *J. Am. Chem. Soc.* **2009**, *131*, 4588–4589.

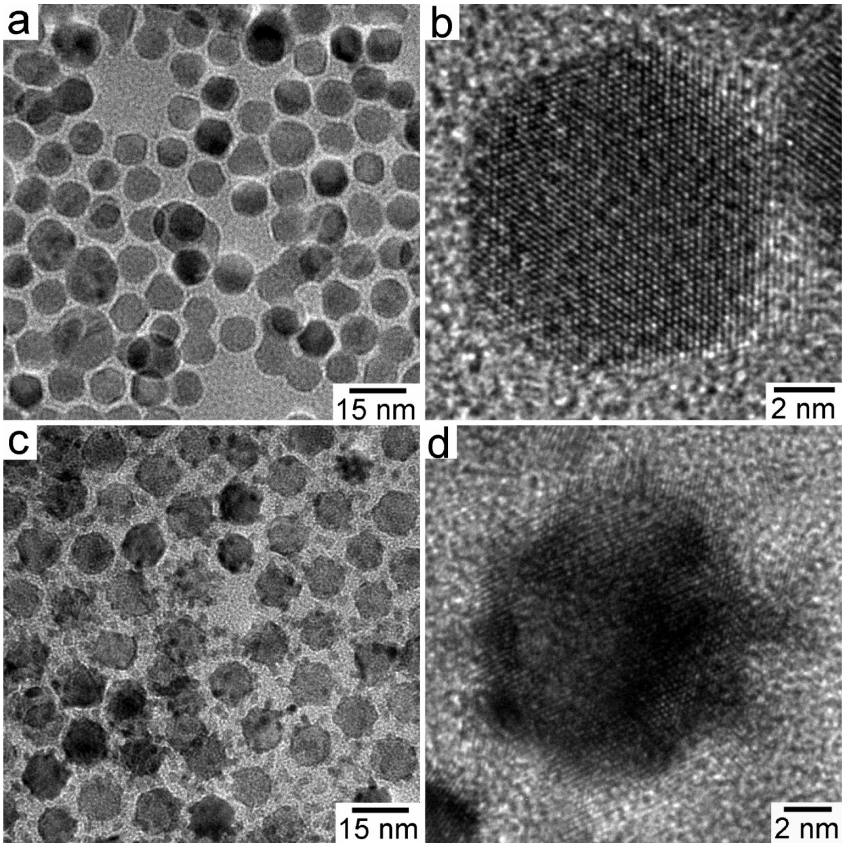

Figure 1. Representative TEM and HR-TEM images of as-prepared (a, b) Ag and (c, d) Pt-on-Ag nanoparticles, respectively.

The three-electrode system consisted of a rotating disk working electrode made of glassy carbon (RDE, 5 mm in diameter), a platinum wire counter electrode, and a hydrogen reference electrode (HydroFlex, Gaskatel). The HydroFlex electrode was calibrated by performing hydrogen evolution reaction (HER) with two Pt electrodes. All the potentials were recorded with respect to a reversible hydrogen electrode (RHE). Five milligrams of acetic acid-treated carbon-supported Pt-on-Ag nanoparticles were dispersed in a mixture of deionized water, isopropanol, and 5 wt % Nafion solution ($V_{water}/V_{2\text{-propanol}}/V_{5\%Nafion} = 0.8/0.2/0.005$), followed by sonication for 10 min. This mixture was deposited onto a RDE and dried under a stream of air. The amount of metals used in the experiment was 0.5 μg unless stated otherwise, which was determined by thermal gravimetric analysis (TGA). A 0.1-M perchloric acid ($HClO_4$) aqueous solution was used as the supporting electrolyte. The potentials for removing silver atoms were monitored using cyclic voltammetry (CV). Before each experiment, the solution was bubbled with argon for 30 min to remove dissolved oxygen. The potential was cycled between 0 and 1.3 V for 20 times at a scan rate of 50 mV/s and a RDE rotating rate of 1600 rpm to complete the dissolution.

Characterization. Transmission electron microscopy (TEM) and high-resolution transmission electron microscopy (HR-TEM) images were taken on a FEI TECNAI F-20 field emission microscope at an accelerating voltage of 200 kV. Scanning transmission electron microscopy (STEM) and elemental maps were carried out under a high-angle annular dark field (HAADF) mode on the same microscope. The optimal resolutions of this microscopy are 1 Å under TEM mode and 1.4 Å under STEM mode. Energy dispersive X-ray (EDX) analysis of particle ensembles was carried out on a field emission scanning electron microscope (FE-SEM, Zeiss-Leo DSM982) installed with an EDAX detector. Powder X-ray diffraction (PXRD) patterns were recorded using a Philips MPD diffractometer with a Cu Kα X-ray source (λ = 1.5405 Å). Ultraviolet−visible (UV−vis) spectra were collected with a UV/vis/NIR spectrometer (Perkin-Elmer Lambda 900). The specimens used for UV−vis study were made by dispersing nanoparticles in toluene. The loading amount of metals on carbon was determined using an SDT-Q600 system from TA Instruments, Inc.

Electrochemical properties were measured on the same electrochemical workstation described above. Carbon-supported platinum (20 wt % Pt, E-tek) was used as a reference catalyst. The protocols for loading this catalyst onto the electrodes followed those described above, and the total amount of the metals used was fixed at 0.5 μg unless stated otherwise. An oxygen-free aqueous solution of $HClO_4$ (0.1 M), which was obtained through degassing with argon for 30 min, was used for the electrochemical active surface area (ECSA) measurement. After 20 cycles, The CV curves were recorded at a scan rate of 50 mV/s and the RDE rotating rate of 1600 rpm unless stated otherwise. All oxygen reduction reaction (ORR) tests were conducted at room temperature in an oxygen-saturated aqueous solution of $HClO_4$ (0.1 M). In all these ORR studies, the loading amount of catalysts was kept at 2 μg based on the amount of metals. The polarization curves were obtained by sweeping the potential from 0 to 1 V at the scan rate of 10 mV/s and rotating speed of 1600 rpm. To evaluate the long-term stability of Pt hollow nanoparticles, an accelerated test was conducted by running 30 000 linear potential sweeps between 0.6 and 1.0 V at a scan rate of 100 mV/s in an argon-protected 0.1-M $HClO_4$ aqueous solution.

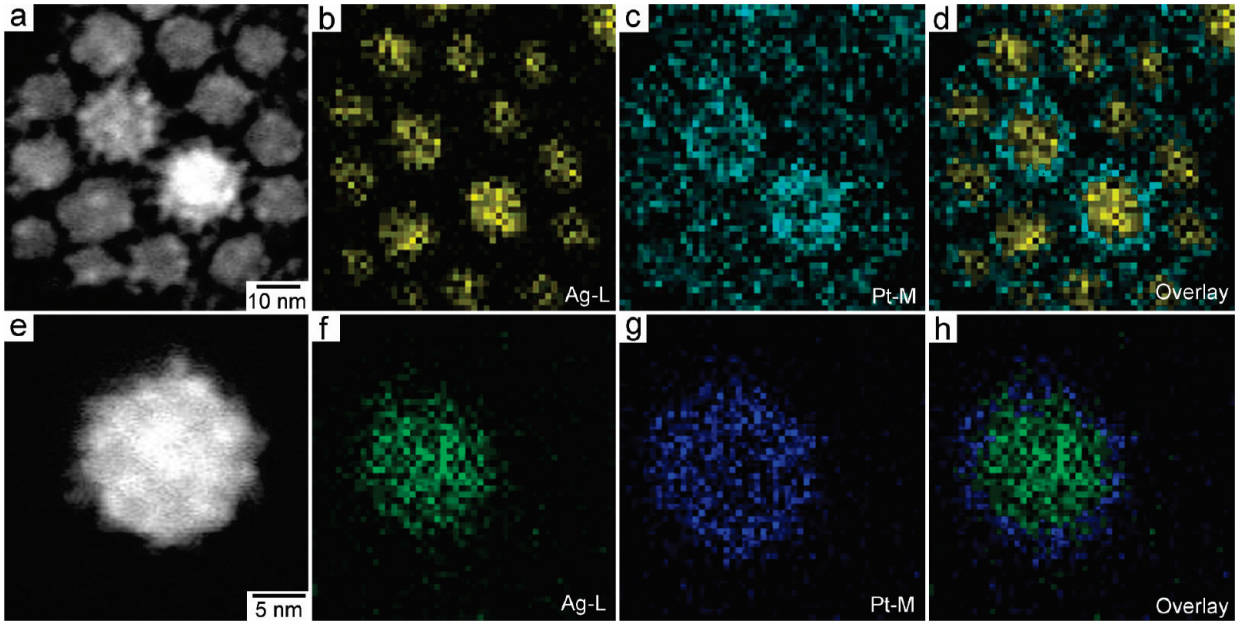

Figure 2. Representative HAADF-STEM images and their corresponding elemental maps of Pt-on-Ag nanoparticles at (a−d) low and (e−h) high magnifications.

Results and Discussion

Figure 1a shows a representative TEM image of as-synthesized silver nanoparticles made by using a procedure published elsewhere.[38] Silver trifluoroacetate was used as the precursor because it has good solubility in various organic solvents and can be thermally reduced to silver metal.[40,41] The silver nanoparticles were fairly uniform and had an average size of 9.5 ± 1.3 nm. HR-TEM studies show that most of the silver nanoparticles had truncated octahedral shape (Figure 1b). These Pt-on-Ag nanoparticles were obtained by reducing $Pt(acac)_2$ at 180 °C at a $Pt(acac)_2$/Ag-nanoparticle molar ratio of one. The reaction took 1 h to complete and oleylamine acted as both reducing and capping agent.[1,42,43] The Ag nanoparticles served as seed crystals for the growth of Pt-on-Ag heteronanostructures and could also assist the platinum reduction process.[44,45] The Ag cores were mostly covered by multiple 3-nm Pt nanoparticles (Figure 1c). Figure 1d shows the HR-TEM image of an individual Pt-on-Ag nanoparticle. The Pt nanoparticles seemed to grow directly on the surfaces of Ag nanoparticles, since no clear discontinuity was observed between their lattices.

The distribution of Ag and Pt in the nanoparticles was studied by EDX analysis using the HAADF-STEM. Figure 2 shows a representative STEM image of Pt-on-Ag nanoparticles and the corresponding Ag and Pt elemental maps. The Ag signal was readily detectable and concentrated in the cores of Pt-on-Ag nanostructures, judging by its distribution with respect to the particles shown in the STEM image (Figure 2b). The distribution of Pt metal was quite different from that of Ag in both location and intensity of the signal (Figure 2c). This difference was more pronounced when their elemental maps were compared using overlays based on the signals from Pt-M and Ag-L lines (Figure 2d). The signals from the Ag were completely surrounded by those from Pt. A careful STEM and EDX study on the individual Pt-on-Ag nanoparticle shows that the particle-on-particle morphology could be observed under the HAADF-STEM mode (Figure 2e). The Ag distributed mostly in central region, suggesting that the core consisted of Ag nanoparticles (Figure 2f). The distribution of Pt, however, looked quite different, with the EDX signals appearing both at the edge and in the center (Figure 2g). These converging data revealed an overgrowth of platinum on the surface of silver nanoparticles as shown in the overlay of the nanoparticle (Figure 2h).

The PXRD patterns were recorded for both as-prepared Ag and Pt-on-Ag nanoparticles (Figure 3a). The diffraction peaks can be indexed to (111), (200), (220), (311), and (222) planes of a face-centered cubic (fcc) structure. The well-defined shape and fairly good intensity of these peaks suggested reasonable crystallinity for both types of nanoparticles. The diffraction peaks became asymmetric, especially in the high-angle region, after Pt was deposited on the Ag nanoparticles. The diffractions from Pt metal were readily detectable and the corresponding XRD patterns can be deconvoluted into two sets of peaks for pure Ag and Pt, respectively. EDX analyses on the ensembles of Pt-on-Ag nanoparticles indicate that these particles had an empirical composition of $Pt_{43}Ag_{57}$, close to the feeding ratio of one between $Pt(acac)_2$ and Ag particle precursors (Figure 3b and Table 1).

(40) Fields, E. K.; Meyerson, S. *J. Org. Chem.* **1976**, *41*, 916–920.
(41) Lin, X. Z.; Teng, X. W.; Yang, H. *Langmuir* **2003**, *19*, 10081–10085.
(42) Capdevielle, P.; Lavigne, A.; Sparfel, D.; Baranne lafont, J.; Cuong, N. K.; Maumy, M. *Tetrahedron Lett.* **1990**, *31*, 3305–3308.
(43) Zhong, X.; Feng, Y.; Lieberwirth, I.; Knoll, W. *Chem. Mater.* **2006**, *18*, 2468–2471.
(44) Song, H.; Kim, F.; Connor, S.; Somorjai, G. A.; Yang, P. D. *J. Phys. Chem. B* **2005**, *109*, 188–193.
(45) Teng, X. W.; Yang, H. *Nano Lett.* **2005**, *5*, 885–891.

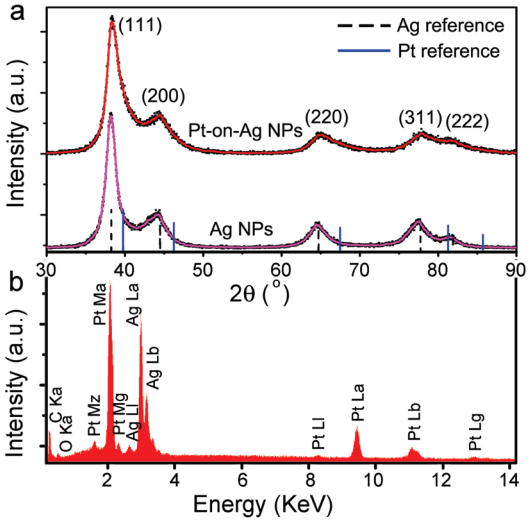

Figure 3. (a) PXRD patterns of as-prepared Ag (bottom) and Pt-on-Ag (top) nanoparticles and (b) the corresponding EDX spectrum for Pt-on-Ag nanoparticles.

Table 1. Summary of Pt-on-Ag Heteronanostructures Prepared under Various Reaction Conditions

sample no.	T (°C)	$Pt(acac)_2$/Ag nanoparticle molar ratio	morphology	atomic composition
1	170	1:1	Pt-on-Ag NPs	$Pt_{14}Ag_{86}$
2	180	1:2	Pt-on-Ag NPs	$Pt_{29}Ag_{71}$
3[a]	180	1:1	Pt-on-Ag NPs	$Pt_{43}Ag_{57}$
4	180	2:1	Pt-on-Ag and free Pt NPs	N/A
5	190	1:1	Pt-on-Ag and free Pt NPs	N/A

[a] The optimal condition for making Pt-on-Ag nanoparticles (NPs), which were used subsequently for preparing Pt hollow structures and Pt-on-Ag and PtAg alloy catalysts.

UV−vis spectroscopy was used to monitor the growth process of Pt-on-Ag nanoparticles by taking out aliquots of the mixtures periodically. Ag nanoparticles are known to have a surface plasmon resonance (SPR) band in the visible range. The intensity of this SPR peak is sensitive to the surface coverage and was used to study the deposition of Pt. Figure 4 shows a series of spectra collected at different reaction times. The pure Ag nanoparticles exhibited a characteristic SPR peak at around 390 nm, close to the values reported.[38,41] The intensity of Ag plasmon band gradually decreased over the reaction time, indicating a gradual increase in the surface coverage by Pt nanoparticles. A weak but detectable peak could still be observed after the reaction for 120 min. This signal was associated with either a small fraction of exposed Ag surface or a damping effect on its SPR due to thin coating layer of Pt.

TEM was used to further study the growth of Pt-on-Ag nanoparticles. No obvious large deposition of Pt on the surface of Ag nanoparticles after the reaction for 2 min (Figure 5a). HR-TEM study, however, shows that there were subtle changes in the morphology and sub-nanometer-sized tiny particles were observed (Figure 5b).

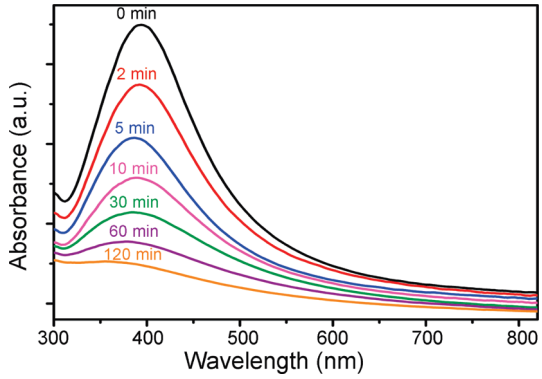

Figure 4. UV−vis spectra of Ag (0 min) and Pt-on-Ag nanoparticles made after the reaction for a time period between 2 and 120 min, respectively.

It seems that Pt nucleated and grew directly on the Ag surfaces. The size of the Pt nanoparticles became sufficiently large for imaging after reaction for 30 min (Figure 5c,d). This growth process continued until the precursors were exhausted after the reaction for about 120 min (Figure 5e,f). The observed particle-on-particle morphology resembled the product formed through either Stranski−Krastanov (SK) or Volmer−Weber (VW) mode.[1,46,47] These growth modes, governed by the interplay between global surface energy and interfacial energy, led to the formation of either island-on-wetting-layer or isolated islands on substrate.

Both the reaction temperature and $Pt(acac)_2$/Ag metal molar ratio were varied systematically to optimize the conditions for the synthesis of Pt-on-Ag nanostructures. Both the population and size of Pt nanoparticles decreased dramatically if the reaction took place at 170 °C for 1 h while keeping the $Pt(acac)_2$/Ag particle precursor ratio at unity (Figure 6a). The resulting products had an appearance overall composition of $Pt_{14}Ag_{86}$, indicating an incomplete reduction of $Pt(acac)_2$. When the reaction temperature was raised to 190 °C while keeping all other conditions the same, a large amount of free Pt nanoparticles formed besides the Pt-on-Ag nanoparticles, indicating that the homogeneous nucleation and growth became possible upon the reduction of $Pt(acac)_2$ under this temperature (Figure 6b).

If the $Pt(acac)_2$/Ag nanoparticle molar ratio was lowered to 1/2 while keeping the reaction at 180 °C for 1 h, the surface coverage of Ag nanoparticles by Pt was reduced, resulting in a composition of $Pt_{29}Ag_{71}$ (Figure 7a). When the $Pt(acac)_2$/Ag nanoparticle molar ratio raised to 2, both Pt-on-Ag and individual free Pt nanoparticles were found (Figure 7b). These results are summarized in Table 1. The correlation between reaction parameters and final product can be understood in terms of reaction kinetics and a competing process between heterogeneous and homogeneous nucleation and growth. Low reaction temperature and $Pt(acac)_2$ concentration favor heterogeneous nucleation and growth since the energy barriers should be lower than that for its competitive process.[1]

(46) Bauer, E.; Vandermerwe, J. H. *Phys. Rev. B* **1986**, *33*, 3657–3671.
(47) Chambers, S. A. *Surf. Sci. Rep.* **2000**, *39*, 105–180.

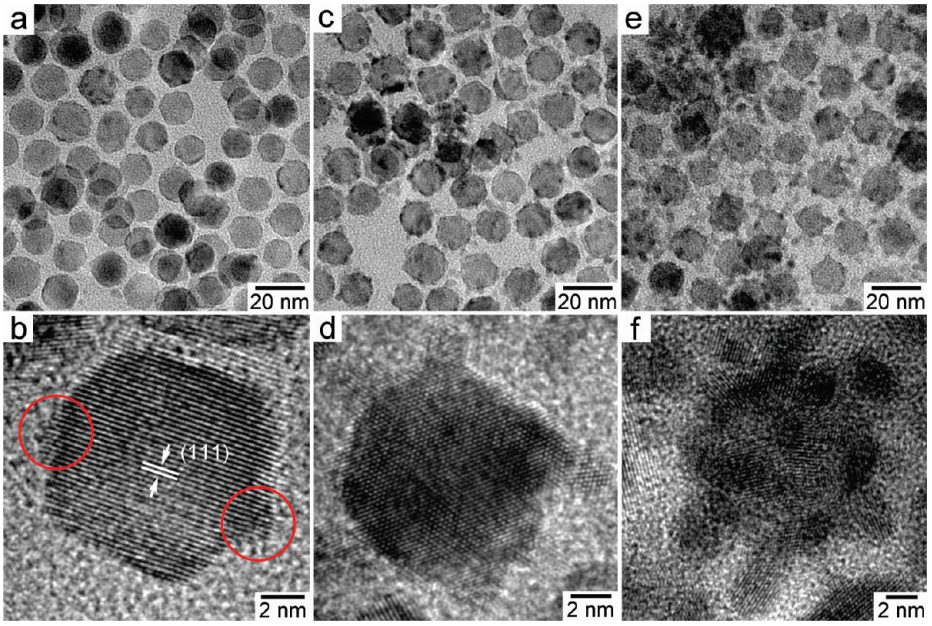

Figure 5. Representative TEM and HR-TEM images of Pt-on-Ag nanoparticles made after the reaction for (a, b) 2, (c, d) 30, and (e, f) 120 min, respectively.

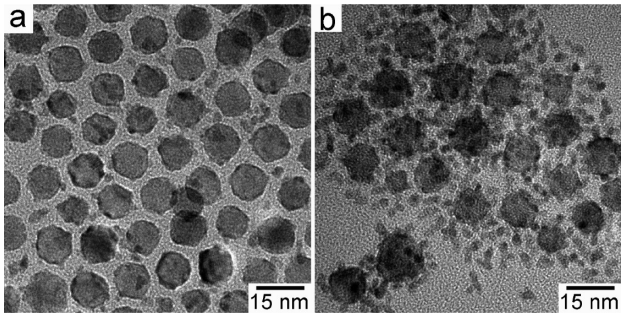

Figure 6. Representative TEM images of Pt-on-Ag nanoparticles made at (a) 170 and (b) 190 °C, respectively. The reaction time was 1 h and $Pt(acac)_2$/Ag metal molar ratio was kept at one.

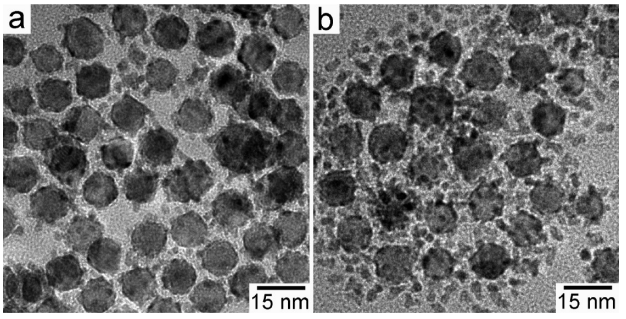

Figure 7. Representative TEM images of Pt-on-Ag nanoparticles made at the $Pt(acac)_2$/Ag metal molar ratio of (a) 1/2 and (b) 2/1, respectively. These reactions took placed at 180 °C for 1 h.

A low reaction temperature also leads to slow reaction kinetics according to the Arrhenius law. The optimal temperature for preparing Pt-on-Ag heteronanostructures with minimum free Pt nanoparticles were experimentally determined to be about 180 °C at a $Pt(acac)_2$/Ag nanoparticle molar ratio of 1/1.

We hypothesized that if the Pt-on-Ag nanoparticles resembled the products formed through the SK or VW growth mode, selective removal of Ag core might be possible to create Pt hollows if the Pt nanocrystals packed sufficiently dense. Such hollow nanostructures could have high specific surface areas and Pt primary particles in the optimal size range for catalyzing oxygen reduction reaction (ORR). Pt-on-Ag and PtAg nanoparticles should not be the choice of catalysts, as incorporation of Ag often lowers the Pt catalytic activity toward ORR due to largely the electronic effect.[23,48,49]

Vulcan carbon was used as the support in this study to minimize the possible aggregation and sintering among the nanoparticles during the treatment. Figure 8a,b shows representative TEM images of carbon-supported Pt-on-Ag nanoparticles. The type of Pt-on-Ag nanoparticles used was made at 180 °C with a $Pt(acac)_2$/Ag metal molar ratio of 1/1 as shown in Figure 1 and had a composition of $Pt_{43}Ag_{57}$. The loading amount was 16.3 wt % of metals on carbon. These Pt-on-Ag nanoparticles were uniformly dispersed on the carbon particles. Treating the particles with acetic acid or at 300 °C in air and then a forming gas of diluted hydrogen in argon were the two methods used to remove the surface capping agents, mostly composed of oleylamine. The morphology of Pt-on-Ag nanoparticles was largely intact after the treatment with acetic acid (Figure 8c,d). The thermal treatment, on the other hand, made the particle surfaces smooth, resulting in the loss of their dendritic structures (Figure 8e,f). Such morphological change is often the results of formation of alloy or other rearrangement processes. Figure 9 shows the PXRD patterns of these two types of products. The XRD pattern of acid-treated sample looked similar to

(48) Greeley, J.; Norskov, J. K.; Mavrikakis, M. *Annu. Rev. Phys. Chem.* **2002**, *53*, 319–348.
(49) Hammer, B.; Norskov, J. K. Theoretical surface science and catalysis - Calculations and concepts. *Advances in Catalysis*; Academic Press Inc.: San Diego, 2000; Vol. *45*, pp 71−129.

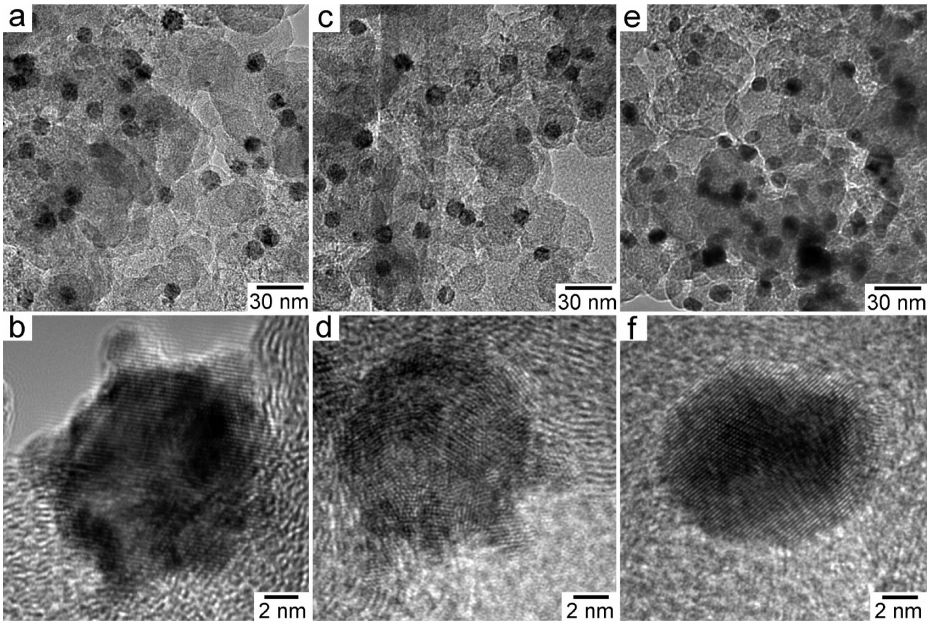

Figure 8. Representative TEM and HR-TEM images of carbon-supported (a, b) Pt-on-Ag nanoparticles, and the resulting products after (c, d) acid and (e, f) thermal treatments.

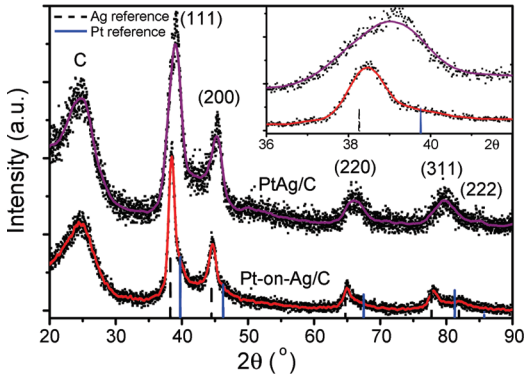

Figure 9. PXRD patterns of acid-treated Pt-on-Ag nanostructures (bottom) and thermally treated PtAg nanoparticles (top). Inset: enlarged region for the (111) diffractions.

the as-prepared Pt-on-Ag nanoparticles and the dominant diffraction was from the (111) plane of the relatively large Ag cores. The diffraction peak at around 25° 2θ was from the graphitic carbon fragments of the carbon support. The (111) diffraction shifted dramatically for the sample with the treatment at 300 °C and fell in between those for pure Pt and Ag metals. Such observation is a strong indication of the formation of PtAg mixed alloys.[50]

Carbon-supported platinum hollow nanostructures were produced from those acetic acid-treated Pt-on-Ag nanoparticles through the electrochemical dissolution of silver cores (Figure 10). The potential range used in this procedure was from 0 to 1.3 V, and the supporting electrolyte was perchloric acid. The upper limit of the scan potential was well above the standard potential of 0.80 V for electrochemical oxidation of Ag metal,[51] and

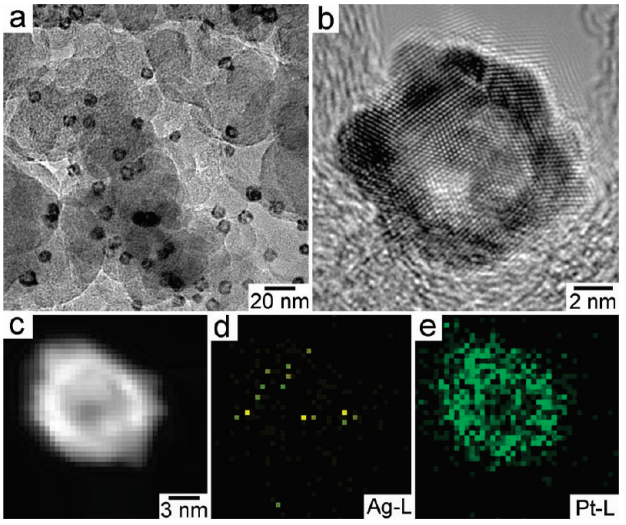

Figure 10. Representative (a) TEM, (b) HR-TEM, and (c) STEM images and (d, e) elemental maps of carbon-supported Pt hollow structures made from carbon-supported Pt-on-Ag nanoparticles.

it should help in removing the organic residues on the particle surfaces after the acetic acid treatment. Figure 10a shows representative TEM images of the hollow particles that had the characteristic contrast difference between the center and edge regions. The HR-TEM image shows that the hollow particles had good crystallinity with clearly visible (111) lattices of fcc phase (Figure 10b). The STEM image and the corresponding elemental maps based on Ag-L and Pt-M lines reveal that the shell of hollow structure was primarily made of Pt, and a negligible amount of Ag was detected (Figure 10c–e). It is worthwhile to point out the fact that the continuous shell of hollow structures that can be produced provides additional proof for a likely Stranski–Krastanov growth mode of Pt on Ag cores.[47] Unlike the products obtained after exposure to acetic acid, PtAg alloy formed after heat treatment. Silver metal could

(50) Peng, Z. M.; Yang, H. *J. Solid State Chem.* **2008**, *181*, 1546–1551.
(51) Lide, D. R. *CRC Handbook of Chemistry and Physics*, 88th ed. (Internet Version 2008); CRC Press/Taylor and Francis: Boca Raton, FL, 2008.

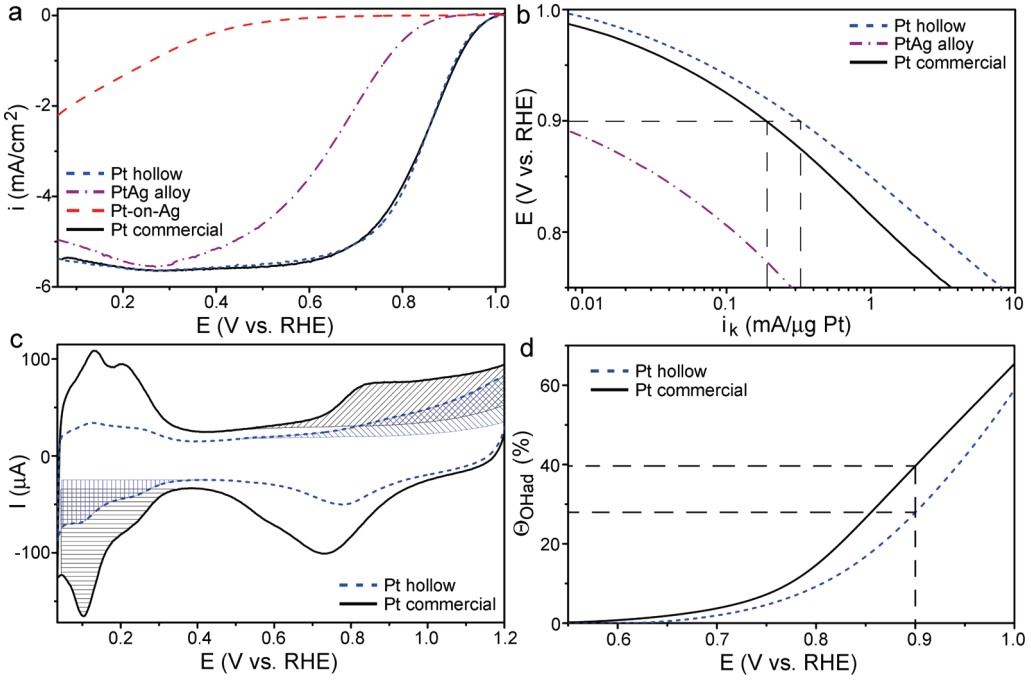

Figure 11. (a) ORR polarization curves, (b) intrinsic mass current density, (c) CV, and (d) hydroxyl surface coverage (Θ_{OHad}) of carbon-supported Pt-on-Ag nanoparticle, PtAg alloy, Pt hollow, and particle reference catalysts.

not be removed electrochemically from these nanoparticles. Both Pt and Ag elements distributed uniformly in such nanoparticles, as shown by the TEM and EDX studies (Supporting Information Figure S1).

Carbon-supported Pt hollow nanoparticles (Pt-hollow), together with Pt-on-Ag, PtAg, and Pt (Pt/C, 20 wt %, E-TEK) catalysts, were studied for their ORR activities. The carbon-supported Pt-on-Ag nanoparticles show little hydrogen adsorption−desorption (HAD, $E < 0.4$ V), indicating that these particles were largely electrochemically inactive. Although the electronic effect due to the incorporation of Ag into Pt could not be ruled out,[48,49] incomplete removal of surface capping agents using acetic acid should be the key factor contributing to the low hydrogen adsorption on Pt-on-Ag nanoparticles, as HAD signals were observed for both PtAg nanoalloys and Pt-hollow structures (Supporting Information Figure S2). The ECSA values were calculated to be 34.6 m^2/g Pt for PtAg nanoalloys and 60.9 m^2/g Pt for Pt-hollow nanostructures. In comparison, the ECSA for the Pt reference from E-tek was 83.5 m^2/g Pt. The relatively high surface area for the commercial Pt catalysts is because of the small particle size.[12]

While it had lower electrochemical surface area than the Pt reference, Pt-hollow nanostructures exhibited significantly higher activity than both Pt and PtAg alloy catalysts in ORR. Figure 11a shows the ORR polarization curves for these four different types of catalysts. The Pt-on-Ag nanostructures were least active, having a detectable onset current below about 0.5 V. The large negative on-set potential shift in comparison to the Pt reference catalyst revealed a poor ORR activity of PtAg catalyst. The ORR polarization curve for Pt hollows almost overlapped with the one for the commercial Pt nanocatalysts, even though these hollow particles had a smaller ECSA and lower Pt loading on the RDE than the Pt reference catalyst.

The intrinsic current densities of these catalysts were calculated by applying the Koutecky−Levich equation,[52,53] which can be depicted as follows:

$$\frac{1}{i} = \frac{1}{i_k} + \frac{1}{i_d} = \frac{1}{i_k} + \frac{1}{B\omega^{1/2}} \qquad (1)$$

where i is the measured current density, i_k is the kinetic current density, i_d is the diffusion (mass-transfer) limited current density, B is a constant which is a function of concentration (C_{O2}) and diffusion coefficient (D_{O2}) of O_2 in the electrolyte and the viscosity of electrolyte (ν), and ω is the rotation rate of the electrode in units of rpm. On the basis of this equation, the Pt hollow catalyst had an intrinsic mass current density of 322 $\mu A/\mu g$ Pt at 0.9 V, almost twice the value of 187 $\mu A/\mu g$ Pt for Pt nanoparticles (Figure 11b). The improvement in area-specified current density was even more pronounced, which was 529 $\mu A/cm^2$ Pt at 0.9 V and over two times of the value of 224 $\mu A/cm^2$ Pt for Pt nanoparticles (Supporting Information Figure S3).[12] Both were significantly higher than the PtAg alloy made from Pt-on-Ag nanoparticles. As indicated above, the low ORR activity of PtAg alloy catalysts can be partially explained in terms of the electronic structures, that is, an upshift in the d-band of Pt due to the interaction with Ag metal.[48,49] Such upshift in d-band structure results in an increase in the coverage of OH group on the catalyst surfaces, which is detrimental to

(52) Bard, A. J.; Faulkner, L. R. *Electrochemical Methods - Fundamentals and Application*; 2nd ed.; John Wiley & Sons: New York, 2001.
(53) Vielstich, W.; Lamm, A.; Gasteiger, H. A. *Handbook of Fuel Cells, Fundamentals Technology and Applications*; John Wiley & Sons Ltd.: New York, 2003; Vol. *2*.

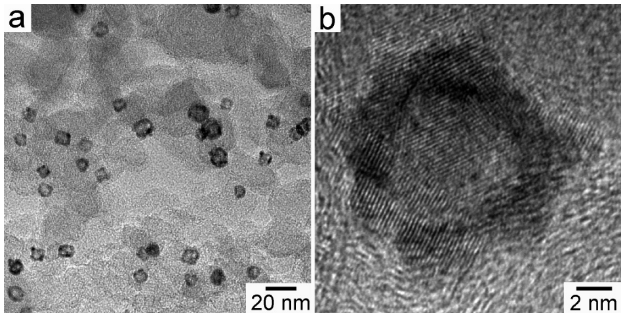

Figure 12. Representative (a) TEM and (b) HR-TEM images of carbon-supported platinum hollow structures after an accelerated electrochemical stability test. Oxidation−reduction cycles were carried out through applying 30 000 linear potential sweeps between 0.6 and 1.0 V.

ORR activity.[8,10] Visible difference in OH coverage was also observed between the Pt hollow and reference catalysts. As shown in Figure 11c, the value of OH coverage is the quotient of OH adsorption area (shaded area on forward sweep between 0.6 and 1.2 V) divided by the overall active surface area (shaded area of backward sweep between ~0.05 and 0.4 V) in the CV curves. The Pt hollow catalyst clearly had a lower OH coverage than that of Pt reference over the entire potential range (Figure 11d). Small size of the Pt primary nanocrystals of a continuous shell could be an important structural factor contributing to this enhancement of ORR activity.[2,10,54] These Pt hollow nanostructures were physically stable after multiple electrochemical cycles. In this accelerated stability test, potential was continuously swept between 0.6 and 1.0 V linearly for 30 000 times in a 0.1-M $HClO_4$ aqueous solution. TEM images show the overall structure of the hollows retained largely intact, although the surface topology changed substantially (Figure 12a). HR-TEM study indicates that the surface of these Pt hollows became smooth and the population of dendrite-like features diminished after the multiple cycles (Figure 12b).

(54) Paulus, U. A.; Wokaun, A.; Scherer, G. G.; Schmidt, T. J.; Stamenkovic, V.; Radmilovic, V.; Markovic, N. M.; Ross, P. N. *J. Phys. Chem. B* **2002**, *106*, 4181–4191.

Conclusions

Pt-on-Ag bimetallic heteronanostructures can be obtained by reducing platinum precursors in the presence of Ag nanoparticles. The formation of Pt-on-Ag nanoparticles is shown to follow a heterogeneous nucleation and growth process resembling the products formed through the Stranski−Krastanov growth mode. Platinum hollow nanostructures can be obtained from Pt-on-Ag nanoparticles using an electrochemical method. The Pt hollow nanostructures are more active than a commercial reference Pt catalyst in the oxygen reduction reaction, suggesting the hollow nanostructures contribute to the enhanced catalytic activity.

Acknowledgment. This work was supported by NSF (DMR-0449849). It made use of Shared Facilities at University of Rochester River Campus EM Lab supported in part by DOE. Z.M.P. is a Hooker Fellowship recipient.

Supporting Information Available: Figures S1−S3 contain TEM, STEM, and EDX analysis of PtAg alloy nanoparticles and CV and area specific current density for ORR catalyzed by carbon-supported catalysts of Pt nanoparticles (Pt reference), hollows, and PtAg alloy nanostructures (PDF). This material is available free of charge via the Internet at http://pubs.acs.org.